Mathematical Biosciences and Engineering

MBE, 20(5): 9288–9304.
DOI: 10.3934/mbe.2023407
Received: 09 November 2022
Revised: 08 February 2023
Accepted: 22 February 2023
Published: 16 March 2023

http://www.aimspress.com/journal/MBE

Research article

RISE-based adaptive control of electro-hydraulic servo system with uncertain compensation

Xiaohan Yang[1], Yinghao Cui[2,*], Zhanhang Yuan[3,4] and Jie Hang[3]

[1] Institute of Information Technology, Information Engineering University, Zhengzhou 450002, China
[2] School of Mechanical & Electronic Engineering, Zhongyuan University of Technology, Zhengzhou 450007, China
[3] School of Automation Science and Electrical Engineering, Beihang University, Beijing 100191, China
[4] China Nuclear Power Engineering Co. LTD, Beijing 100840, China

* **Correspondence:** Email: yh_cui@zut.edu.cn.

Abstract: Electro-hydraulic servo system (EHSS) plays an important role in many industrial and military applications. However, its high-performance tracking control is still a challenging mission due to its nonlinear system dynamics and model uncertainties. In this paper, a novel adaptive robust integral method of the sign of the error (ARISE) with extended state observer (ESO) is proposed. Firstly, the nonlinear mathematical model of typical EHSS with modeling uncurtains and uncertain nonlinear is established. Then, ESO is used to estimate the state and lumped disturbance, of which the unknown parameter estimations can be updated by the novel adaptive law. Results shows that the novel controller achieves better tracking performance in maximum tracking error, average tracking error and standard deviation of the tracking error.

Keywords: electro-hydraulic system; extended state observer; parameter estimation, adaptive error sign integral robust controller; trajectory tracking

Nomenclature

A_p	Ram area
C_t	Internal leakage coefficient
P_1, P_2,	Oil pressures inside the chambers of the actuator, respectively
P_L	Load pressure
P_r	Return pressure
P_s	Supply pressure
Q_1, Q_2	Oil flow in both chambers of the actuator
V_{01}, V_{02}	Initial volume of oil inlet and outlet chamber, respectively
V_1, V_2	Control volume of oil inlet and outlet chamber, respectively
f_v	Damping coefficient
g_1, g_2	Pressure difference of inlet and outlet
k	Spring stiffness
k_1, k_2,k_3, k_r	Positive gains
k_t	Total gain of the servo valve
m_p	Mass of load
q_1, q_2	Model errors because of internal leakage
u	Control voltage
x_p	Position of load
β	Gain
β_{e1}, β_{e2}	Oil effective bulk modulus of the actuator, respectively
ω	Bandwidth of the extended state observer
ARISE	Adaptive robust integral of the sign of the error
ESO	Extended state observer
RISE	Robust integral of the sign of the error

1. Introduction

Electric hydraulic servo system (EHSS) is widely used in industry applications due to its high power ratio and fast response [1–6]. With the rapid development of technology, more severe control requirements are put forward for EHSS, and high-performance control becomes eagerly needed to address its behavioral nonlinearity and uncertainties, such as flow nonlinearity, pressure dynamic nonlinearity, uncertain parameters, unmolded nonlinearity, and external disturbances [7–10].

Nowadays, many researchers focus on advanced control strategies such as robust adaptive control [11,12], sliding mode control [13,14], back-stepping control [15,16], robust integral of the sign of the error (RISE) [17,18] for EHSS. Yue and Yao [17] proposed an adaptive robust integral of the sign of the error control (ARISE), which can adjust the robust gain online through adaptive method to solve the potential high gain feedback of symbolic function. Yao et al. [19] designed a novel ARSE to address noise pollution in the acquisition of acceleration signal, which can compensate the error of friction model and other bounded disturbances [20]. The above literature shows that RISE/ARISE control greatly improves the trajectory tracking accuracy of EHSS. However, those controllers regard the parameter adaptive error, unmolded error, and external disturbance as lumped disturbance, which severely limits the control accuracy. Control strategy based on disturbance observer can compensate the influence of disturbance and uncurtains effectively, which has been used in the field of control

theory and engineering [21–26]. Especially, the extended state observer (ESO), which is the core of ADRC and has been widely used in disturbance estimation and suppression [27–32].

In this paper, the sign function is replaced with a modified arctangent function to smooth the nonlinearity of sign function. Then, the state and external disturbance can be estimated by ESO, respectively. Finally, the residual observation error is compensated to further enhance the tracking accuracy by ARISE. The Lyapunov theory proves the EHSS can achieve asymptotic s. Simulation results show the proposed controller has a better performance in maxi-mum tracking error, average tracking error and standard deviation of the tracking error.

2. Dynamic model of electro-hydraulic servo system

The typical working principle of EHSS is shown in Figure 1. The double rod symmetrical hydraulic cylinder is controlled by servo valve to drive the load.

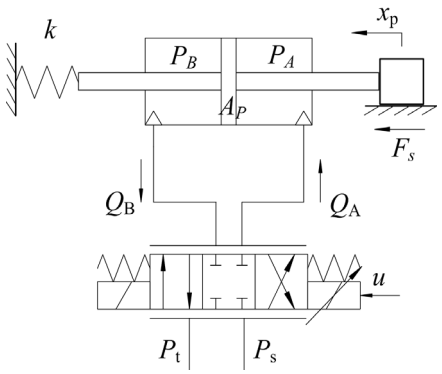

Figure 1. Model of valve controlled symmetrical cylinder system.

In this paper, the force balance equation of EHSS can be given as

$$m_p\ddot{x}_p = P_L A_p - kx_p - f_v\dot{x}_p + f\left(x_p, \dot{x}_p, t\right) \tag{1}$$

where m_p and x_p represent mass and displacement of load respectively; P_L is the pressure difference; A_p is the effective area of the piston; k is the spring stiffness; f_v is the combined coefficient; $f\left(x_p, \dot{x}_p, t\right)$ indicates the lumped uncertain; Pressure dynamics of the two chambers are given by [15].

$$\begin{cases} \dot{P}_1 = \beta_{e1}/V_1\left(Q_1 - A_p\dot{x}_p - C_t P_L + q_1(t)\right) \\ \dot{P}_2 = \beta_{e2}/V_2\left(A_p\dot{x}_p + C_t P_L - Q_2 - q_2(t)\right) \end{cases} \tag{2}$$

where

$$\begin{cases} Q_1 = k_t g_1\left(P_1, x_v\right)u \\ Q_2 = k_t g_2\left(P_2, x_v\right)u \end{cases} \tag{3}$$

$$\begin{cases} g_1 = \sqrt{(P_s - P_t + (P_s - 2P_1 + P_t)\cdot s(u))/2} \\ g_2 = \sqrt{(P_s - P_t - (P_s - 2P_2 + P_t)\cdot s(u))/2} \end{cases} \tag{4}$$

The pressure difference dynamics between the two chambers is expressed as follows

$$\dot{P}_{\mathrm{L}} = \beta_e k_t \left(g_1/V_1 + g_2/V_2\right)u - \beta_e A_{\mathrm{p}} \left(1/V_1 + 1/V_2\right)\dot{x}_{\mathrm{p}} - \beta_e C_{\mathrm{t}} \left(1/V_1 + 1/V_2\right)P_{\mathrm{L}} + \beta_e \left(q_1/V_1 + q_2/V_2\right) \tag{5}$$

where β_{e1}, β_{e2} are the effective elastic modulus in two chamber and $\beta_{e1} = \beta_{e2} = \beta_e$; $V_1 = V_{01} + A_{\mathrm{p}}$; $V_2 = V_{02} - A_{\mathrm{p}} \cdot x_{\mathrm{p}}$ represents the control volume of return chamber; V_{01} and V_{02} are the initial volumes of the two chambers respectively; C_t is the internal leakage coefficient of the cylinder; Q_1 (t) and Q_2 (t) are the oil flowrate of the two chamber of the cylinder respectively; $q_1(t)$ and $q_2(t)$ are model errors because of internal leakage in the two chambers; g_1 is the pressure difference at the oil inlet and g_2 is the pressure difference at the oil outlet; P_s is the supplied pressure; P_r is the return pressure, k_{t} is the total gain of the servo valve; u is the control voltage and $s(u)$ is expressed as

$$s(u) = \begin{cases} 1 & u > 0 \\ 0 & u = 0 \\ -1 & u < 0 \end{cases} \tag{6}$$

To make it smooth and differentiable, the sign function $s(u)$ is replaced by Eq (7).

$$f_{\arctan}(u) = 2\arctan(Ku)/\pi \tag{7}$$

Thus, g_1, g_2 in Eq (4) can be rewritten as Eq (8).

$$\begin{cases} g_1^{'} = \sqrt{(P_s - P_t + (P_s - 2P_1 + P_t) \cdot f_{\arctan}(u))/2} \\ g_2^{'} = \sqrt{(P_s - P_t - (P_s - 2P_2 + P_t) \cdot f_{\arctan}(u))/2} \end{cases} \tag{8}$$

Substituting Eqs (2)–(5) into Eq (1), and thus

$$\begin{aligned} m_{\mathrm{p}}\ddot{x}_{\mathrm{p}} = {} & A_{\mathrm{p}}\beta_e k_t \left(g_1/V_1 + g_2/V_2\right)u - A_{\mathrm{p}}^2\beta_e \left(1/V_1 + 1/V_2\right)\dot{x}_{\mathrm{p}} - A_{\mathrm{p}}\beta_e C_{\mathrm{t}} \left(1/V_1 + 1/V_2\right)P_{\mathrm{L}} + \\ & A_{\mathrm{p}}\beta_e \left(q_1/V_1 + q_2/V_2\right) - k\dot{x}_{\mathrm{p}} - f_{\mathrm{v}}\ddot{x}_{\mathrm{p}} + \dot{f} \end{aligned} \tag{9}$$

Rewritten Eq (9), and thus,

$$\begin{aligned} m_{\mathrm{p}}\ddot{x}_{\mathrm{p}} = {} & A_{\mathrm{p}}\beta_e k_t \left(g_1^{'}/V_1 + g_2^{'}/V_2\right)u - A_{\mathrm{p}}^2\beta_e \left(1/V_1 + 1/V_2\right)\dot{x}_{\mathrm{p}} - A_{\mathrm{p}}\beta_e C_{\mathrm{t}} \left(1/V_1 + 1/V_2\right)P_{\mathrm{L}} + \\ & A_{\mathrm{p}}\beta_e \left(q_1/V_1 + q_2/V_2\right) - k\dot{x}_{\mathrm{p}} - f_{\mathrm{v}}\ddot{x}_{\mathrm{p}} + \dot{f} + f^{'} \end{aligned} \tag{10}$$

where $f^{'}$ is the approximation error caused by using the continuously differentiable function farctan(u).

According to Eq (1)

$$P_{\mathrm{L}} = \frac{m_{\mathrm{p}}}{A_{\mathrm{p}}}\ddot{x}_{\mathrm{p}} + \frac{k}{A_{\mathrm{p}}}x_{\mathrm{p}} + \frac{f_{\mathrm{v}}}{A_{\mathrm{p}}}\dot{x}_{\mathrm{p}} - \frac{f}{A_{\mathrm{p}}} \tag{11}$$

Substituting Eq (11) into Eq (10), thus

$$\begin{aligned} m_{\mathrm{p}}\ddot{x}_{\mathrm{p}} = {} & A_{\mathrm{p}}\beta_e k_t \left(g_1^{'}/V_1 + g_2^{'}/V_2\right)u - \beta_e C_{\mathrm{t}} \left(1/V_1 + 1/V_2\right)kx_{\mathrm{p}} - \left(A_{\mathrm{p}}^2\beta_e \left(1/V_1 + 1/V_2\right) + f_{\mathrm{v}}\beta_e C_{\mathrm{t}} \left(1/V_1 + 1/V_2\right) + k\right)\dot{x}_{\mathrm{p}} - \\ & \left(m_{\mathrm{p}}\beta_e C_{\mathrm{t}} \left(1/V_1 + 1/V_2\right) + f_{\mathrm{v}}\right)\ddot{x}_{\mathrm{p}} + \beta_e C_{\mathrm{t}} \left(1/V_1 + 1/V_2\right)f + \dot{f} + f^{'} + A_{\mathrm{p}}\beta_e \left(q_1/V_1 + q_2/V_2\right) \end{aligned} \tag{12}$$

Define state variables as $\boldsymbol{x} = \left[x_1, x_2, x_3\right]^{\mathrm{T}} = \left[x_{\mathrm{p}}, \dot{x}_{\mathrm{p}}, \ddot{x}_{\mathrm{p}}\right]^{\mathrm{T}}$ and output variables as $y = x_1 = x_{\mathrm{p}}$, so the state space model of EHSS can be expressed as

$$\begin{cases} \dot{x}_1 = x_2 \\ \dot{x}_2 = x_3 \\ \dot{x}_3 = \theta_1 u - \theta_2 x_1 - \theta_3 x_2 - \theta_4 x_3 + \Delta \end{cases} \tag{13}$$

where $\theta_1 = A_p \beta_e k_t \left(\frac{g_1^{'}}{V_1} + \frac{g_1^{'}}{V_2} \right) \Big/ m_p$, $\theta_2 = \beta_e C_t \left(\frac{1}{V_1} + \frac{1}{V_2} \right) k \Big/ m_p$, $\theta_3 = \left(A_p^2 \beta_e \left(\frac{1}{V_1} + \frac{1}{V_2} \right) + f_v \beta_e C_t \left(\frac{1}{V_1} + \frac{1}{V_2} \right) + k \right) \Big/ m_p$, $\theta_4 = \left(m_p \beta_e C_t \left(\frac{1}{V_1} + \frac{1}{V_2} \right) + f_v \right) \Big/ m_p$, $\Delta = \left(\beta_e C_t \left(\frac{1}{V_1} + \frac{1}{V_2} \right) f + \dot{f} + f^{'} + A_p \beta_e \left(\frac{q_1}{V_1} + \frac{q_1}{V_2} \right) \right) \Big/ m_p$.

In practice, the parameters m, k, β_e and C_t may not be known accurately, so it is necessary to consider the uncertainties of these parameters. Define vector as $\boldsymbol{\theta} = [\theta_1, \theta_2, \theta_3, \theta_4]$ and improve the tracking performance of the system through the adaptive method.

The purpose of the system controller is to design a bounded control input u so that $y = x_1$ can track the desired trajectory $y_d(t) = x_{1d}(t)$. Therefore, the following assumptions should be given.

***Assumption* 1**: The desired trajectory x_{1d} is five times differentiable and each is bounded. In practice, the load pressure of hydraulic cylinder meets $0 < P_L < P_s$.

***Assumption* 2**: The range of parametric uncertainties is

$$\theta \in \Omega_\theta \tag{14}$$

$$\Omega_\theta \triangleq \{\theta : \theta_{\min} \le \theta \le \theta_{\max}\} \tag{15}$$

where $\theta_{\min} = [\theta_{1\min}, \cdots, \theta_{4\min}]^T$, $\theta_{\max} = [\theta_{1\max}, \cdots, \theta_{4\max}]^T$ are known.

***Assumption* 3**: The time-varying perturbation $\Delta(t)$ of Eq (10) is smooth enough so that

$$|\dot{\Delta}(t)| \le \delta_1 \ \& \ |\ddot{\Delta}(t)| \le \delta_2 \tag{16}$$

where δ_1, δ_2 are known positive constants.

3. Extend state observer design

ESO can estimate the uncertainty disturbance comprehensively, so we use ESO to estimate the lumped disturbance and compensate it feed forward to achieve better tracking accuracy.

Define $x_4 = \Delta(t)$, $\dot{x}_4 = \delta(t)$ and the expanded state space can be written as

$$\begin{cases} \dot{x}_1 = x_2 \\ \dot{x}_2 = x_3 \\ \dot{x}_3 = \theta_1 u - \theta_2 x_1 - \theta_3 x_2 - \theta_4 x_3 + x_4 \\ \dot{x}_4 = \delta \end{cases} \tag{17}$$

Defining $\tilde{x} = x - \hat{x}$ as the estimation error of x, where $\hat{x}$ represents the estimated value of x.

According to the expanded state space model, the ESO is designed as

$$\begin{cases} \dot{\hat{x}}_1 = \hat{x}_2 + 4\omega_0 (x_1 - \hat{x}_1) \\ \dot{\hat{x}}_2 = \hat{x}_3 + 6\omega_0^2 (x_1 - \hat{x}_1) \\ \dot{\hat{x}}_3 = \hat{\theta}_1 u - \hat{\theta}_2 x_1 - \hat{\theta}_3 x_2 - \hat{\theta}_3 x_3 + \hat{x}_4 + 4\omega_0^3 (x_1 - \hat{x}_1) \\ \dot{\hat{x}}_4 = \omega_0^4 (x_1 - \hat{x}_1) \end{cases} \tag{18}$$

where ω_0 is the bandwidth of the extended state observer, $\hat{\theta}_i$ is the estimated value of the unknown parameters θ_i, I = 1, 2, 3, 4.

The dynamic equation of observation error can be obtained by subtracting Eq (17) an Eq (18):

$$\begin{cases} \dot{\tilde{x}}_1 = \tilde{x}_2 - 4\varpi_0 \tilde{x}_1 \\ \dot{\tilde{x}}_2 = \tilde{x}_3 - 6\omega_0^2 \tilde{x}_1 \\ \dot{\tilde{x}}_3 = \tilde{x}_4 + \tilde{\boldsymbol{\theta}}^{\mathrm{T}} \boldsymbol{\Phi}_1 - 4\omega_0^3 \tilde{x}_1 \\ \dot{\tilde{x}}_4 = \delta - \omega_0^4 \tilde{x}_1 \end{cases} \tag{19}$$

where $\tilde{\boldsymbol{\theta}} = \left[\tilde{\theta}_1, \tilde{\theta}_2, \tilde{\theta}_3, \tilde{\theta}_4\right]^{\mathrm{T}}$, $\boldsymbol{\Phi}_1 = \left[u, x_1, x_2, x_3, x_4\right]^{\mathrm{T}}$.

Let

$$\xi_i = \frac{\tilde{x}_i}{\omega_0^{i-1}}, i = 1,2,3,4 \tag{20}$$

Then Eq (17) can be written as

$$\begin{bmatrix} \dot{\xi}_1 \\ \dot{\xi}_2 \\ \dot{\xi}_3 \\ \dot{\xi}_4 \end{bmatrix} = \varpi_0 \underbrace{\begin{bmatrix} -4 & 1 & 0 & 0 \\ -6 & 0 & 1 & 0 \\ -4 & 0 & 0 & 1 \\ -1 & 0 & 0 & 0 \end{bmatrix}}_{\boldsymbol{A}} \begin{bmatrix} \xi_1 \\ \xi_2 \\ \xi_3 \\ \xi_4 \end{bmatrix} + \underbrace{\begin{bmatrix} 0 \\ 0 \\ 1 \\ 0 \end{bmatrix}}_{B_1} \frac{\tilde{\theta}^T \Phi}{\varpi_0^2} + \underbrace{\begin{bmatrix} 0 \\ 0 \\ 0 \\ 1 \end{bmatrix}}_{B_2} \frac{\delta}{\varpi_0^3} \tag{21}$$

$$\dot{\xi} = \omega_0 \boldsymbol{A} \xi + \boldsymbol{B}_1 \frac{\tilde{\boldsymbol{\theta}}^{\mathrm{T}} \boldsymbol{\Phi}}{\omega_0^2} + \boldsymbol{B}_2 \frac{\delta}{\varpi_0^3} \tag{22}$$

Since matrix $\boldsymbol{A}$ is a Hurwitz matrix, and there is a positive definite symmetric matrix $\boldsymbol{P}$ which satisfies the following equation

$$\boldsymbol{A}^{\mathrm{T}} \boldsymbol{P} + \boldsymbol{P} \boldsymbol{A} = -\boldsymbol{I} \tag{23}$$

The symmetric positive definite matrix $\boldsymbol{P}$ is:

$$\boldsymbol{P} = \begin{bmatrix} 17/8 & -1/2 & -11/8 & 1/2 \\ -1/2 & 11/8 & -1/2 & -17/8 \\ -11/8 & -1/2 & 17/8 & -1/2 \\ 1/2 & -17/8 & -1/2 & 91/8 \end{bmatrix}$$

4. Projection mapping and parameter adaptation

Considering Eq (14) and Eq (15), the discontinuous projection can be defined as [11].

$$\mathrm{Proj}_{\hat{\alpha}_i}(\cdot_i) = \begin{cases} 0, \cdot_i > 0 & \text{and} \, \hat{\alpha}_i = \alpha_{i\max} \\ 0, \cdot_i < 0 & \text{and} \, \hat{\alpha}_i = \alpha_{i\min} \\ \cdot_i, & \text{otherwise} \end{cases} \tag{24}$$

where $\hat{\alpha}$ denote the estimate of α and $\tilde{\alpha}$ denote the estimate error, $\tilde{\alpha} = \hat{\alpha} - \alpha$, i =1, 2, 3, 4.

Using the adaptation law as follow:

$$\dot{\hat{\alpha}} = \mathrm{Proj}_{\hat{\alpha}}(\Gamma\tau(t)),\ \hat{\alpha}(0) = \Omega_{\hat{\alpha}} \tag{25}$$

where Γ is the diagonal positive definite adaptation rate matrix, τ is an adaptation function. For any adaption function τ, the adaptation Eq (25) satisfies follow [3]:

$$\hat{\alpha} \in \Omega_{\hat{\alpha}} \triangleq \left\{\hat{\alpha} : \alpha_{\max} \le \hat{\alpha} \le \alpha_{\min}\right\} \tag{26}$$

$$\tilde{\alpha}^T[\Gamma^{-1}\mathrm{Proj}_{\hat{\alpha}}(\Gamma\tau) - \tau] \le 0,\ \forall\tau \tag{27}$$

5. Design of adaptive robust integral of the sign of the error controller

Defining the following error variables

$$\begin{cases} z_1 = x_1 - x_{1\mathrm{d}}, z_2 = \dot{z}_1 + k_1 z_1 \\ z_3 = \dot{z}_2 + k_2 z_2, r = \dot{z}_3 + k_3 z_3 \end{cases} \tag{28}$$

where $x_{1\mathrm{d}}$ is the given trajectory; k_1 k_2 k_3 are the positive feedback gain and r is the auxiliary error signal. Because r contains the differentiation of acceleration, it is considered to be unmeasurable in practice and only used for auxiliary design. According to Eq (28), r has the following expansion:

$$\begin{aligned} r = {} & \theta_1 u - \theta_2 x_{1\mathrm{d}} - \theta_3 \dot{x}_{1\mathrm{d}} - \theta_4 \ddot{x}_{1\mathrm{d}} + \Delta - \dddot{x}_{1\mathrm{d}} - \left(\theta_2 - k_1\theta_3 - k_1^3 + \theta_4 k_1^2\right) z_1 - \\ & \left(k_1^2 + k_1 k_2 - k_2^2\theta_3 - \theta_4 k_1 - \theta_4 k_2\right) z_2 + \left(k_1 + k_2 + k_3 - \theta_4\right) z_3 \end{aligned} \tag{29}$$

Dividing Eq (29) by θ_1, and thus

$$\begin{aligned} \alpha_1 r = {} & u - \alpha_1 \dddot{x}_{1\mathrm{d}} - \alpha_2 x_{1\mathrm{d}} - \alpha_3 \dot{x}_{1\mathrm{d}} - \alpha_4 \ddot{x}_{1\mathrm{d}} + \alpha_1\Delta - \left(\alpha_2 - k_1\alpha_3 - \alpha_1 k_1^3 + \alpha_4 k_1^2\right) z_1 - \\ & \left(\left(k_1^2 + k_1 k_2\right)\alpha_1 - k_2^2\alpha_3 - \alpha_4 k_1 - \alpha_4 k_2\right) z_2 + \left(\left(k_1 + k_2 + k_3\right)\alpha_1 - \alpha_4\right) z_3 \end{aligned} \tag{30}$$

where $\alpha_1 = 1/\theta_1$, $\alpha_2 = \theta_2/\theta_1$, $\alpha_3 = \theta_3/\theta_1$, $\alpha_4 = \theta_4/\theta_1$.

The model-based controller is designed as follows:

$$\begin{cases} u = u_a + u_s, u_s = \left(u_{s1} + u_{s2}\right), u_{s1} = -k_3 z_3 \\ u_{s2} = -k_r z_3 + k_r z_3(0) - \int_o^t \left[k_r k_3 z_3(\tau) + \beta S(z_3(\tau))\right] \mathrm{d}\tau \\ u_a = \hat{\alpha}_1 \dddot{x}_{1\mathrm{d}} + \hat{\alpha}_2 x_{1\mathrm{d}} + \hat{\alpha}_3 \dot{x}_{1\mathrm{d}} + \hat{\alpha}_4 \ddot{x}_{1\mathrm{d}} - \hat{\alpha}_1\hat{\Delta} = \hat{\alpha}^{\mathrm{T}}\boldsymbol{\Phi}_2 - \hat{\alpha}_1\hat{\Delta} \end{cases} \tag{31}$$

where $\hat{\boldsymbol{\alpha}} = [\hat{\alpha}_1, \hat{\alpha}_2, \hat{\alpha}_3, \hat{\alpha}_4]^{\mathrm{T}}$ represents the estimated value of $\boldsymbol{\alpha} = [\alpha_1, \alpha_2, \alpha_3, \alpha_4]^{\mathrm{T}}$; $k_r > 0$ is the gain of controller; $\beta > 0$ is the robust gain; u_a is the feedforward model compensation, u_{s1} is the linear robust feedback term, u_{s2} is the RISE control term, $\boldsymbol{\Phi}_2 = [\ddot{x}_{1\mathrm{d}}, x_{1\mathrm{d}}, \dot{x}_{1\mathrm{d}}, \ddot{x}_{1\mathrm{d}}]^{\mathrm{T}}$.

Substituting Eq (31) into Eq (30) and note that $d = -\hat{\alpha}_1\hat{\Delta} + \alpha_1\Delta$

$$\alpha_1 r = \tilde{\boldsymbol{\alpha}}^{\mathrm{T}}\boldsymbol{\Phi}_2 + d - \left(k_3 + k_r\right) z_3 + k_r z_3(0) - \int_o^t \left[k_r k_3 z_3(\tau) + \beta S(z_3(\tau))\right] \mathrm{d}\tau - A z_1 - B z_2 + C z_3 \tag{32}$$

$\tilde{\boldsymbol{\alpha}} = \hat{\boldsymbol{\alpha}} - \boldsymbol{\alpha}$, Substitute Eq (25) into Eq (32), thus

$$\alpha_1 \dot{r} = \mathrm{Proj}_{\hat{\alpha}}(\Gamma\tau)^T \boldsymbol{\Phi}_2 + \tilde{\boldsymbol{\alpha}}^{\mathrm{T}}\dot{\boldsymbol{\Phi}}_2 + \dot{d} - \left(k_3 + k_r - C\right) r - \beta S\left(z_3\right) + A k_1 z_1 - \left(A - B k_2\right) z_2 - \left(B + C k_3\right) z_3 \tag{33}$$

The overall structure of the designed control strategy is shown in Figure 2.

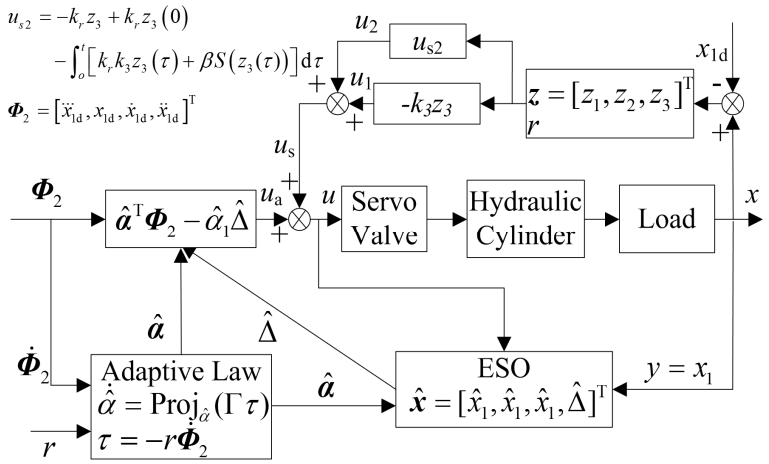

Figure 2. Overview of control diagram.

Lemma 1: Define variable *L(t)* as

$$L(t) = r\left[\dot{d} - \beta \text{sign}(z_3)\right] \tag{34}$$

Define auxiliary function as

$$P(t) = \beta |z_3(0)| - z_3(0)\dot{d} - \int_0^t L(v) dv \tag{35}$$

According to [8], if the gain β satisfies the following inequality, then the auxiliary function *P(t)* is always positive definite.

$$\beta \geq \delta_1 + \frac{1}{k_3}\delta_2 \tag{36}$$

Theorem 1: Using the adaptive law Eq (25), and adaptive function $\tau = -r\dot{\Phi}_2$, and the robust gain β satisfies inequality Eq (36) as well as the feedback gains k_1, k_2, k_3, k_r are sufficient to ensure that the matrix Λ defined below is positive definite, the adaptive robust integral of the sign of the error controller Eq (31) can make all signals bounded in the closed-loop system, and the system obtains asymptotic output tracking, i.e., $z_1 \to 0$ as $t \to \infty$.

$$\Lambda = \begin{bmatrix} k_1 & -\frac{1}{2} & 0 & -\frac{1}{2}k_5 \\ -\frac{1}{2} & k_2 & -\frac{1}{2} & -\frac{1}{2}k_6 \\ 0 & -\frac{1}{2} & k_3 & -\frac{1}{2}k_{67} \\ -\frac{1}{2}k_5 & -\frac{1}{2}k_6 & -\frac{1}{2}k_7 & k_4 \end{bmatrix} \tag{37}$$

where $k_4 = \max\left(\dot{\Phi}_2^T \Gamma \Phi_2\right) + k_3 + k_r - C$, $k_5 = Ak_1$, $k_6 = -(A - Bk_2)$, $k_7 = -(B + Ck_3)$, $\max(\cdot)$ represents the maximum value of the matrix.

Proof: see Appendix A.

6. Simulation validation

The nominal value of the physical parameters of the valve controlled symmetrical hydraulic cylinder are shows in Table 1. The following controllers are compared by simulation to validate the effectiveness of the designed controller.

Table 1. Physical parameters of the valve controlled symmetrical hydraulic cylinder.

Parameter	Value	Unit	Parameter	Value	Unit
m_p	0.76167	kg	f_v	100	N/(m/s)
A_p	2.5×10^{-4}	m^2	V_{10}	1×10^{-3}	m^3
k	10900	N/m	V_{20}	1×10^{-3}	m^3
β_e	2×10^8	Pa	k_t	5.656×10^{-8}	$m^3/(s \cdot V \cdot N^{1/2})$
C_t	1×10^{-13}	$m^3/(Pa \cdot s)$	q_1	1×10^{-12}	m^3/s
q_2	1×10^{-12}	m^3/s	C_d	0.7	
C_v	1	/	W_p	5	e^{-3}
Δp	821,993	/	α	69	°
K	1000				

(1) Controller I: ESO based ARISE This is the controller designed in this paper. The controller parameters are selected as: $k_1 = 200$, $k_2 = 180$, $k_3 = 0.08$, $k_r = 0.012$, $\beta = 0.05$, $\omega = 100$. According to the nominal value of the parameters, the estimated boundary of unknown parameter α are given as: $\alpha_{min} = [5 \times 10^{-5}\ 0.03\ 2.5\ 8 \times 10^{-3}]$ and $\alpha_{max} = [7 \times 10^{-5}\ 0.07\ 3.5\ 20.2 \times 10^{-3}]$. The initial estimates of α is set as $\hat{\alpha}(0) = [6.5 \times 10^{-5}\ 0.04\ 3\ 8.2 \times 10^{-3}]$ and Γ is set as diag$[1 \times 10^{-15}\ 2 \times 10^{-2}\ 0.001\ 5 \times 10^{-10}]$.

(2) Controller II: ARISE without ESO. Compared to the controller II, there is no ESO compensation term and the other parameters are same to controller I. That is only u_α in Eq (18) is replaced as: $u_a = \hat{\alpha}_1 \ddot{x}_{1d} + \hat{\alpha}_2 x_{1d} + \hat{\alpha}_3 \dot{x}_{1d} + \hat{\alpha}_4 \ddot{x}_{1d} = \hat{\alpha}^T \boldsymbol{\Phi}_2$

(3) Controller III: PI controller. The parameters are set as $k_P = 410$ and $k_I = 10$, which are the optimal solutions after repeated debugging.

(4) Controller IV: BP neutral network PID controller. The structure of the neutral network is 3-5-3, and the learning rate $\eta = 0.28$, inertia coefficient $\alpha = 0.3$.

The desired trajectories are designed as three cases: normal motion with the motion trajectory $x_d(t) = 10\arctan[\sin(\pi t)](1 - e^{-t})/0.7854$ mm, fast level motion with the motion trajectory $x_d(t) = 10\arctan[\sin(4\pi t)](1 - e^{-t})/0.7854$ mm and low-level motion with the motion trajectory $x_d(t) = 10\arctan[\sin(0.2\pi t)](1 - e^{-t})/0.7854$ mm. The external disturbance is designed as $f(t) = 20\arctan[\sin(0.8\pi t)](1 - e^{-t})/0.7854$ N.

To compare the tracking responses of each controller quantitatively, three performance indices including maximum absolute value of the tracking error M_e, average tracking error μ_e, standard deviation of the tracking error σ_e, which were defined in are adopted to evaluate [20].

(1) Case I-normal level motion

The four controllers are tested for a normal motion trajectory $x_d(t)$ = 10arctan[sin(πt)] [1-exp(-t)]/0.7854 mm. The tracking performance are shown in Figures 4–6, the performance indices of the

four controllers is shown in Table 2. From the Figures 4–6 and Table 1, it is obviously that the valve controlled symmetrical cylinder has the best tracking performance under the controller designed in this paper than other controllers. From Table 2, the amplitudes of steady-state tracking error of the controller III and controller IV are both about 0.6 mm, while controller I is about 0.003 mm and controller II is about 0.01 mm, it shows that the ARISE can deal with nonlinear and uncertainties and disturbance well but PI controller just has some robustness. By comparing the performance indices in Table 2 and tracking error in Figure 6 of controller I and controller II, it can be seen that controller I is better than controller II in all indices obviously, which indicates that the parameter adaptation in Figure 6 and ESO compensates for both parametric and uncertain lumped disturbance are effective. The control input u of controller I showed in Figure 3 is continuous and smooth, which makes it easy to implement in practice.

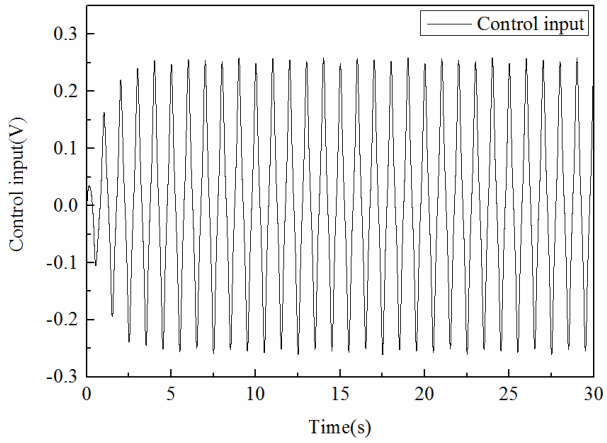

Figure 3. Tracking performance of controller I for normal level motion.

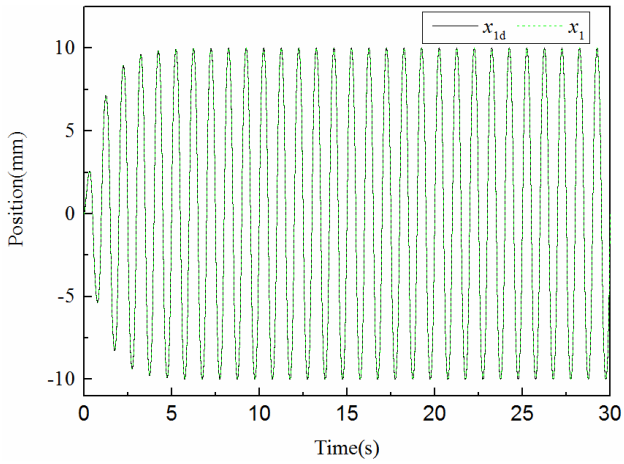

Figure 4. Tracking performance of controller I for normal level motion.

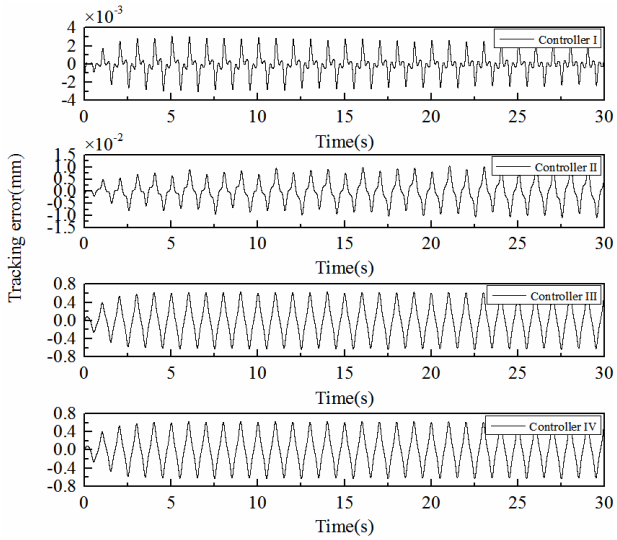

Figure 5. Tracking errors of four controllers I for normal level motion.

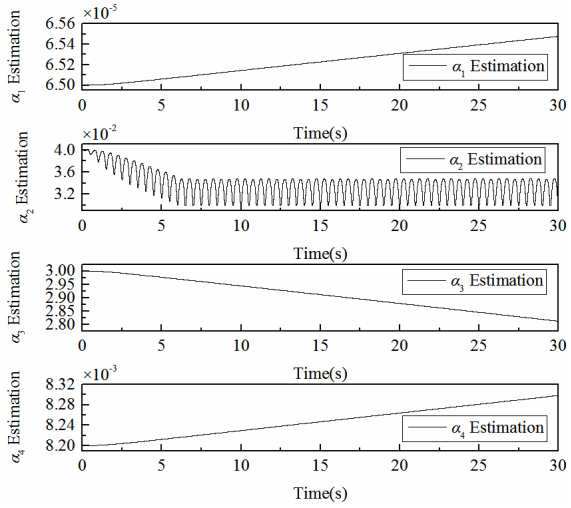

Figure 6. Parameter adaptation of controller I.

Table 2. Performance indices during the last two cycles for normal motion case.

Indices	M_e (mm)	μ_e (mm)	σ_e (mm)
controller I	0.00304985	0.000778897	0.00084379
controller II	0.010971	0.00364635	0.00293964
controller III	0.63097	0.299917	0.197092
controller IV	0.630986	0.299916	0.197092

(2) Case II-low level motion

In this case, a low level reference trajectory $x_d(t)$ = 10arctan[sin(0.2πt)][1-exp(-t)]/0.7854 mm is tested. The results are shown in Figures 7–9 and the performance indices are listed in Table 3. From Figure 7 and Table 3, the amplitudes of steady-state tracking error of the controller III and controller IV are both about 0.076mm, while controller I and controller II both are about 9.5 × 10^{-5} mm, which shows that the ARISE can also deal with nonlinear and uncertainties and disturbance well in low level

reference trajectory. By comparing the performance indices of controller I and controller II in Table 3, it can be seen that the maximum absolute value of the tracking error M_e of the two controllers almost the same, but the average tracking error μ_e, and standard deviation of the tracking error σ_e of controller I are 6.536×10^{-6} mm and 8.833×10^{-6} mm respectively which are better than that of 2.87371×10^{-5} and 1.02822×10^{-5} of controller II obviously, which further validates the effectiveness of the desired parameter adaptation and ESO compensation. The parameter adaptation of controller I are omitted. The control input u of controller I showed in Figure 8 is continuous and there is slight high-frequency vibration. So the controller designed in this paper has the best tracking performance on low level reference trajectory than other controllers too.

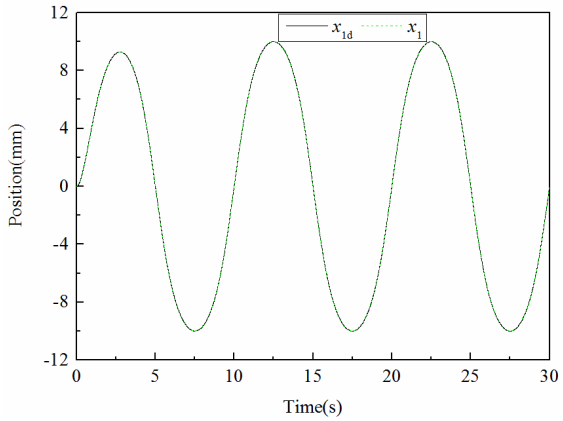

Figure 7. Tracking performance of controller I for low level motion.

Table 3. Performance indices during the last two cycles for slow motion case.

Indices	M_e(mm)	μ_e(mm)	σ_e(mm)
controller I	9.508×10^{-5}	6.536×10^{-6}	8.833×10^{-6}
controller II	9.58784×10^{-5}	2.87371×10^{-5}	1.02822×10^{-5}
controller III	7.5716×10^{-2}	3.14012×10^{-2}	2.00589×10^{-2}
controller IV	7.57345×10^{-2}	3.13926×10^{-2}	2.00719×10^{-2}

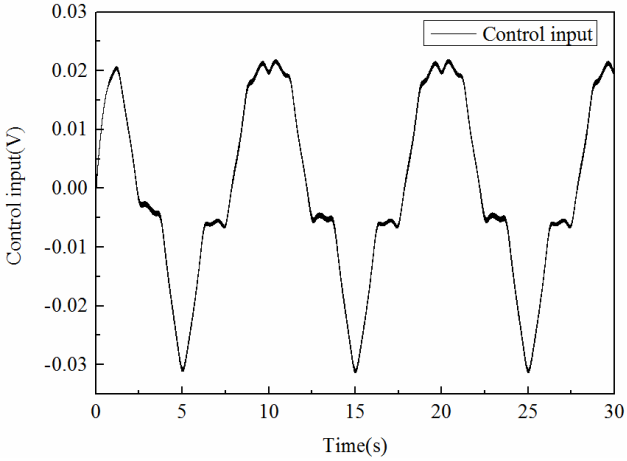

Figure 8. Control input of controller I for normal level motion.

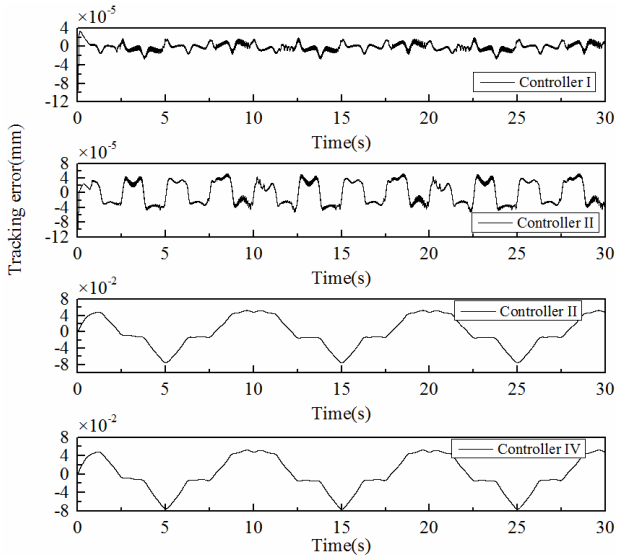

Figure 9. Tracking errors of four controllers I for low level motion.

(3) Case III-fast level motion

A faster level reference trajectory $x_d(t) = 10\arctan[\sin(4\pi t)][1-\exp(-t)]/0.7854$ mm is tested in this case. The results are shown in Figured 10–12 and the performance indices are listed in Table 4. From Figure 12 and Table 4, the amplitudes of steady-state tracking error of the controller III and controller IV are both about 1.24 mm, while controller I 1.34×10^{-2} mm and controller II 4.20256×10^{-2} mm, which shows that the ARISE can better deal with nonlinear and uncertainties and disturbance in fast level reference trajectory than PI controller too. In addition, comparing the performance indices of controller I and controller II in Table 4, it can be seen that the maximum absolute value of the average tracking error μ_e of the controller I is 4.14×10^{-3} mm and the controller II is 1.63032×10^{-2} mm, the standard deviation of the tracking error σ_e of controller I are 5.53×10^{-3} mm and the controller II is 1.30355×10^{-2} mm. These further validate the effectiveness of the desired parameter adaptation and ESO compensation. The control input u of controller I showed in Figure 11 is continuous and smooth. The result verifies that the controller designed in this paper still has high tracking accuracy in tracking performance on fast level reference trajectory.

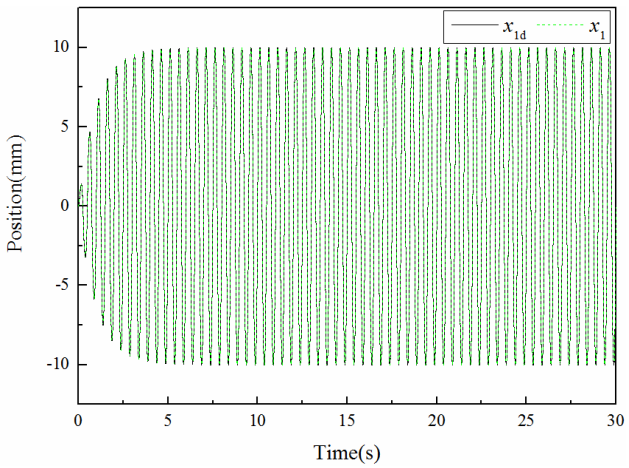

Figure 10. Tracking performance of control-ler I for fast level motion.

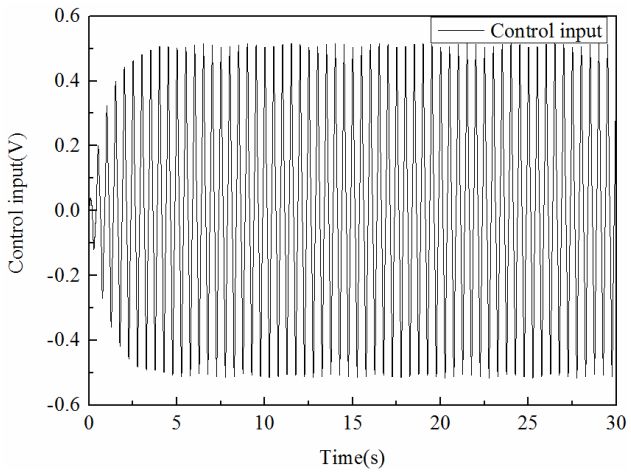

Figure 11. Control input of controller I for normal level motion.

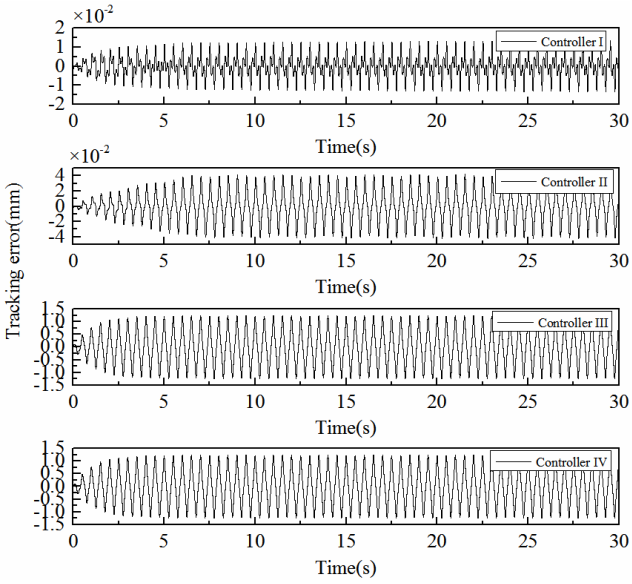

Figure 12. Tracking errors of four controllers I for fast level motion.

Table 4. Performance indices during the last two cycles for fast motion case.

Indices	M_e(mm)	μ_e(mm)	σ_e(mm)
controller I	1.34×10^{-2}	4.14×10^{-3}	5.53×10^{-3}
controller II	4.20256×10^{-2}	1.63032×10^{-2}	1.30355×10^{-2}
controller III	1.238558	0.598359	0.391225
controller IV	1.238657	0.598359	0.391224

7. Conclusions

In this paper, an ARISE with ESO controller is proposed for EHSS to address parametric uncertainties, uncertainty nonlinearities and unmolded disturbances. The proposed ARISE can compensate the dynamics uncertainties, thus guaranteeing asymptotic tracking and improving the adaptability and safety of EHSS. ESO can effectively estimate the state and lumped uncurtains.

Simulation results shows that ARISE with ESO can obtain high tracking accuracy and better performance in tracking desired trajectory under all working conditions.

Conflict of interest

The authors declare there is no conflict of interest.

References

1. Z. X. Jiao, J. X. Gao, Q. Hua, S. P. Wang, The velocity synchronizing control on the electro-hydraulic load simulator, *Chin. J. Aeronaut*., **17** (2004), 39–46. https://doi.org/10.1016/s1000-9361(11)60201-x
2. J. Koivumäki, J. Mattila, Stability-guaranteed impedance control of hydraulic robotic manipulators, *IEEE-ASME Trans. Mech*., **22** (2017), 601–612. https://doi.org/10.1109/tmech.2016.2618912
3. Y. H. Li, Z. L. Wang, Exact linearzization control for the displacement type of actuator with electrical and compound adjustment, *Chin. J. Mech.*, **40** (2004), 21–25. https://doi.org/10.3321/j.issn:0577-6686.2004.11.005
4. J. M. Ma, Y. L. Fu, J. Li, B. Gao, Design simulation and analysis of integrated electrical hydrostatic actuator, *Acta Aeronaut. Astronaut. Sin.*, **26** (2005), 79–83.
5. W. C. Sun, H. H. Pan, H. J. Gao, Filter-based adaptive vibration control for active vehicle suspensions with electrohydraulic actuators, *IEEE Trans. Veh. Technol.*, **65** (2016), 4619–4626. https://doi.org/10.1109/TVT.2015.2437455
6. M. Law, M. Wabner, A. Colditz, M. Kolouch, S. Noack, S. Ihlenfeldt, Active vibration isolation of machine tools using an electro-hydraulic actuator, *CIRP J. Manuf. Sci. Technol.*, **10** (2015), 36–48. https://doi.org/10.1016/j.cirpj.2015.05.005
7. H. E. Merritt, *Hydraulic Control Systems*, New York: Wiley, 1967
8. B. Xian, D. M. Damson, M. S. de Queiroz, J. Chen, A continuous asymptotic tracking control strategy for uncertain nonlinear systems, *IEEE Trans. Autom. Control.*, **49** (2004), 1206–1211. https://doi.org/10.1109/TAC.2004.831148
9. J. Y. Yao, Z. X. Jiao, D. W. Ma, L. Yan, High-accuracy tracking control of hydraulic rotary actuators with modeling uncertainties, *IEEE-ASME Trans. Mech.*, **19** (2014), 633–641. https://doi.org/10.1109/tmech.2013.2252360
10. P. M. Patre, W. MacKunis, C. Makkar, W. E. Dixon, Asymptotic tracking for systems with structured and unstructured uncertainties, in *Proceedings of the 45th IEEE Conference on Decision and Control*, (2006), 441–446. https://doi.org/10.1109/cdc.2006.377377
11. B. Yao, F. Bu, J. Reedy, G. T. C. Chiu, Adaptive robust motion control of single-rod hydraulic actuators: theory and experiments, *IEEE-ASME Trans. Mech.*, **5** (2000), 79–91. https://doi.org/10.1109/3516.828592
12. A. Mohanty, B. Yao, Indirect adaptive robust control of hydraulic manipulators with accurate parameter estimates, *IEEE Trans. Control Syst. Technol.*, **19** (2011), 567–575. https://doi.org/10.1109/tcst.2010.2048569

13. J. Yang, J. Y. Su, S. H. Li, X. H. Yu, High-order mismatched disturbance compensation for motion control systems via a continuous dynamic sliding-mode approach, *IEEE Trans. Ind. Inf.*, **10** (2014), 604–614. https://doi.org/10.1109/tii.2013.2279232
14. D. Won, W. Kim, M. Tomizuka, High gain observer based integral sliding mode control for position tracking of electro-hydraulic servo systems, *IEEE-ASME Trans. Mech.*, **22** (2017), 2695–2704. https://doi.org/10.1109/tmech.2017.2764110
15. J. Y. Yao, Z. X. Jiao, D. W. Ma, Extended-state-observer-based output feedback nonlinear robust control of hydraulic systems with backstepping, *IEEE Trans. Ind. Electron.*, **61** (2014), 6285–6293. https://doi.org/10.1109/TIE.2014.2304912
16. W. Sun, H. J. Gao, O. Kaynak, Adaptive backstepping control for active suspension systems with hard constraints, *IEEE-ASME Trans. Mech.*, **18** (2013), 1072–1079. https://doi.org/10.1109/tmech.2012.2204765
17. X. Yue, J. Y. Yao, Adaptive integral robust control of electro-hydraulic load simulator, *Chin. Hydraul. Pneumatics*, **12** (2016), 25–30. https://doi.org/10.11832 /j.issn.1000-4858.2016.12.004
18. X. Yue, J. Y. Yao, Integral robust based asymptotic tracking control of electro-hydraulic load simulator, *Acta Aeronaut. Astronaut. Sin.*, **38** (2017), 294–303. https://doi.org/10.7527/S1000-6893.2016.0152
19. J. Y. Yao, W. X. Deng, Z. X. Jiao, RISE-based adaptive control of hydraulic systems with asymptotic tracking, *IEEE Trans. Autom. Sci. Eng.*, **14** (2017), 1524–1531. https://doi.org/10.1109/TASE.2015.2434393
20. S. B. Wang, J. Na, X. M. Ren, RISE-based adaptive asymptotic prescribed performance tracking control of nonlinear servo mechanisms, *IEEE Trans. Syst. Man Cybern. Syst.*, **48** (2018), 2359–2370. https://doi.org/10.1109/TSMC.2017.2769683
21. W. Bu, T. Li, J. Yang, Y. Yi, Disturbance observer-based event-triggered tracking control of networked robot manipulator, *Meas. Control.*, **3** (2020), 1–7. https://doi.org/10.1177/0020294020911084
22. H. Rojas-Cubides, J. Cortés-Romero, J. Arcos-Legarda, Data-driven disturbance observer-based control: an active disturbance rejection approach, *Control. Theory Technol.*, **19** (2021), 80–93. https://doi.org/10.1007/s11768-021-00039-x
23. H. F. Li, Y. C. Wang, H. G. Zhang, Data-driven-based event-triggered tracking control for non-linear systems with unknown disturbance, *IET Control. Theory Appl.*, **14** (2019), 2197–2206. https://doi.org/10.1049/iet-cta.2019.0051
24. S. Li, H. Ren, C. Lu, Event-triggered adaptive fault-tolerant control for multi-agent systems with unknown disturbances, *Discrete Contin. Dyn. A*, **8** (2021): 1941–1956. https://doi.org/10.3934/dcdss.2020379
25. X. M. Yao, J. H. Park, L. G. Wu, L. Guo, Disturbance-observer-based composite hierarchical antidisturbance control for singular Markovian jump systems, *IEEE Trans. Autom. Control*, **64** (2019), 2875–2882. https://doi.org/10.1109/TAC.2018.2867607
26. X. M. Yao, L. Guo, Composite anti-disturbance control for Markovian jump nonlinear systems via disturbance observer, *Automatica*, **49** (2013), 2538–2545. https://doi.org/10.1016/j.automatica.2013.05.002
27. J. Q. Han, From PID technique to active disturbances rejection control technique, *Control Eng. China*, **9** (2002), 13–18. https://doi.org/10.14107/j.cnki.kzgc.2002.03.003

28. X. F. Zeng, X. H. Wang, J. Zhang, G. Z. Shen, Disturbance compensated terminal sliding mode control for hypersonic vehicles, *J. Beijing Univ. Aeronaut. Astronaut.*, **38** (2012), 1454–1458. https://doi.org/10.13700/j.bh.1001-5965.2012.11.007
29. Z. J. Kang, X. Chen, Z. L. Cui, H. G. Yu, Bus voltage control method of DC distribution network based on ESO and terminal sliding mode control, *Proc. CSEE*, **38** (2012), 3235–3243. https://doi.org/10.13334/j.0258-8013.pcsee.171197
30. L. Jin, S. J. Xu, Extended state observer based fault detection and recovery for flywheels, *J. Beijing Univ. Aeronaut. Astronaut.*, **34** (2008), 1272–1275. https://doi.org/10.13700/j.bh.1001-5965.2008.11.013
31. C. L. Xia, J. H. Liu, W. Yu, Z. Q. Li, Variable structure control of BLDCM based on extended state observer, in *IEEE International Conference Mechatronics and Automation*, **2** (2005), 568–571. https://doi.org/10.1109/icma.2005.1626612
32. H. Hang, Y. H. Li, L. M, Yang, A novel low pressure-difference fluctuation electro-hydraulic large flowrate control valve for fuel flowrate control of aeroengine afterburner system, *Chin. J. Aeronaut.*, **11** (2021), 363–376. https://doi.org/10.1016/j.cja.2021.07.002

Appendix A

Define a Lyapunov function

$$V = \frac{1}{2}z_1^2 + \frac{1}{2}z_2^2 + \frac{1}{2}z_3^2 + \frac{1}{2}\alpha_1 r^2 + \frac{1}{2}\tilde{\boldsymbol{\alpha}}^{\mathrm{T}}\boldsymbol{\Gamma}^{-1}\tilde{\boldsymbol{\alpha}} + P \tag{A.1}$$

It is Obvious that V is positive definite. The derivative of V is:

$$\dot{V} = z_1\dot{z}_1 + z_2\dot{z}_2 + z_3\dot{z}_3 + \alpha_1 r\dot{r} + \tilde{\boldsymbol{\alpha}}^{\mathrm{T}}\boldsymbol{\Gamma}^{-1}\dot{\hat{\boldsymbol{\alpha}}} + \dot{P} \tag{A.2}$$

Substituting Eqs (25) and (28), L(t)and P(t), into Eq (A.2).

$$\begin{aligned}
\dot{V} &= z_1(z_2 - k_1 z_1) + z_2(z_3 - k_2 z_2) + z_3(r - k_3 z_3) + \\
&\quad r\left\{-\dot{\boldsymbol{\Phi}}_2^{\mathrm{T}}\boldsymbol{\Gamma}\boldsymbol{\Phi}_2 r + \tilde{\boldsymbol{\alpha}}^{\mathrm{T}}\dot{\boldsymbol{\Phi}}_2 + \dot{d} - (k_3 + k_r - C)r - \beta\,\mathrm{sign}(z_3) + Ak_1 z_1 - (A - Bk_2)z_2 - (B + Ck_3)z_3\right\} \\
&\quad + \tilde{\boldsymbol{\alpha}}^{T}\boldsymbol{\Gamma}^{-1}\mathrm{Proj}_{\hat{\theta}}(\Gamma\tau) - r\left[\dot{d} - \beta\,\mathrm{sign}(z_3)\right] \\
&\le z_1(z_2 - k_1 z_1) + z_2(z_3 - k_2 z_2) + z_3(r - k_3 z_3) + \\
&\quad r\left\{-\dot{\boldsymbol{\Phi}}_2^{\mathrm{T}}\boldsymbol{\Gamma}\boldsymbol{\Phi}_2 r + \tilde{\boldsymbol{\alpha}}^{\mathrm{T}}\dot{\boldsymbol{\Phi}}_2 + \dot{d} - (k_3 + k_r - C)r - \beta\,\mathrm{sign}(z_3) + Ak_1 z_1 - (A - Bk_2)z_2 - (B + Ck_3)z_3\right\} \\
&\quad + \tilde{\boldsymbol{\alpha}}^{T}\tau - r\left[\dot{d} - \beta\,\mathrm{sign}(z_3)\right] \\
&= -k_1 z_1^2 - k_2 z_2^2 - k_3 z_3^2 - \left(\dot{\boldsymbol{\Phi}}_2^{\mathrm{T}}\boldsymbol{\Gamma}\boldsymbol{\Phi}_2 + k_3 + k_r - C\right)r^2 + z_1 z_2 + z_2 z_3 + z_3 r + (Ak_1 z_1 - Az_2)r + Bk_2 z_2 r - (B + Ck_3)z_3 r \\
&\triangleq -\boldsymbol{\eta}^{\mathrm{T}}\boldsymbol{\Lambda}\boldsymbol{\eta} \le -\lambda_{\min}(\boldsymbol{\Lambda})\left(z_1^2 + z_2^2 + z_3^2 + r^2\right) \triangleq -W
\end{aligned} \tag{A.3}$$

where $\boldsymbol{\eta} = [z_1, z_2, z_3, r]^{\mathrm{T}}$, $\lambda_{\min}(\boldsymbol{\Lambda})$ is the minimum eigenvalue of matrix $\boldsymbol{\Lambda}$, therefore $V \in L_\infty$ and $W \in L_2$, so z_1, z_2, z_3 and r are bounded. According to the assumptions 1 and 2, all states of the system are bounded so the actual control input u is bounded. According to Eqs (28) and (33), the derivative of W is bounded, so W is uniformly continuous. According to Barbarat's lemma, $W \to 0$ as $t \to \infty$, so the conclusion of the theorem 1 can be deduced, theorem 1 is proofed.